



CrossMark
click for updates

Research

Cite this article: Ortega-Jimenez VM, Sapir N, Wolf M, Variano EA, Dudley R. 2014 Into turbulent air: size-dependent effects of von Kármán vortex streets on hummingbird flight kinematics and energetics. *Proc. R. Soc. B* **281**: 20140180.
<http://dx.doi.org/10.1098/rspb.2014.0180>

Received: 23 January 2014

Accepted: 26 February 2014

Subject Areas:

biomechanics, physiology, ecology

Keywords:

Calypte anna, flight energetics, stability, turbulence, vortex shedding, wingbeat kinematics

Author for correspondence:

Victor M. Ortega-Jimenez

e-mail: vortega@berkeley.edu

†These authors contributed equally to this study.

Electronic supplementary material is available at <http://dx.doi.org/10.1098/rspb.2014.0180> or via <http://rspb.royalsocietypublishing.org>.

Into turbulent air: size-dependent effects of von Kármán vortex streets on hummingbird flight kinematics and energetics

Victor M. Ortega-Jimenez^{1,†}, Nir Sapir^{1,†}, Marta Wolf¹, Evan A. Variano² and Robert Dudley^{1,3}

¹Department of Integrative Biology, and ²Department of Civil and Environmental Engineering, University of California, Berkeley, CA 94720, USA

³Smithsonian Tropical Research Institute, Balboa, Republic of Panama

Animal fliers frequently move through a variety of perturbed flows during their daily aerial routines. However, the extent to which these perturbations influence flight control and energetic expenditure is essentially unknown. Here, we evaluate the kinematic and metabolic consequences of flight within variably sized vortex shedding flows using five Anna's hummingbirds feeding from an artificial flower in steady control flow and within vortex wakes produced behind vertical cylinders. Tests were conducted at three horizontal airspeeds (3, 6 and 9 m s⁻¹) and using three different wake-generating cylinders (with diameters equal to 38, 77 and 173% of birds' wing length). Only minimal effects on wing and body kinematics were demonstrated for flight behind the smallest cylinder, whereas flight behind the medium-sized cylinder resulted in significant increases in the variances of wingbeat frequency, and variances of body orientation, especially at higher airspeeds. Metabolic rate was, however, unchanged relative to that of unperturbed flight. Hummingbirds flying within the vortex street behind the largest cylinder exhibited highest increases in variances of wingbeat frequency, and of body roll, pitch and yaw amplitudes at all measured airspeeds. Impressively, metabolic rate under this last condition increased by up to 25% compared with control flights. Cylinder wakes sufficiently large to interact with both wings can thus strongly affect stability in flight, eliciting compensatory kinematic changes with a consequent increase in flight metabolic costs. Our findings suggest that vortical flows frequently encountered by aerial taxa in diverse environments may impose substantial energetic costs.

1. Introduction

Natural winds present a range of perturbed airflows at various spatio-temporal scales (e.g. turbulence and vortex shedding). The effects of such variability on animal flight performance have been understudied relative to steady flow conditions. Tucker [1] found no effects of small airspeed fluctuations (i.e. 0.88–1.44% RMS/mean values) on seagull flight metabolism. Subsequent studies of avian flight have typically emphasized the low-turbulence characteristics of wind tunnels used in research [2,3]. Orchid bees in fairly turbulent airflow (i.e. approx. 10%) extend their hind legs to increase moment of inertia in roll and to enhance flight stability [4], but other kinematic responses of volant taxa, together with potentially elevated metabolic costs, are unclear. Maximum flight speeds of orchid bees in turbulent airstreams are also reduced relative to low-turbulence conditions at equivalent free-stream airspeeds [4], suggesting that sustained flow perturbation may limit flight stability and other key features of flight performance. Increased kinematic variance, together with associated increases in energetic expenditure, are likely correlates of such aerodynamic challenges.

One interesting case of high-variance flow is the von Kármán vortex street produced by steady flow interrupted by a stationary bluff body. At Reynolds numbers (Re) greater than 10^2 , this condition results in periodic shedding of vortices of alternate rotational sense. These vortices travel far downstream and can form patches of turbulence within them [5]. Von Kármán vortices may thus challenge animal flight control. In water, fish routinely encounter such vortex streets behind obstacles [6]. In response, salmonids, for example, perform phase-matched body displacements that reduce energy costs when station-keeping behind an obstacle's wake [7,8]. In air, environmental flows through vegetation produce complex and irregular flow fields owing to the interaction of wakes from different plant elements, and some flying animals must cope with this complexity [9]. Interestingly, von Kármán vortex streets persist as a dominant flow structure within vegetational canopies [10], even amidst the complexity of interacting wakes, and thus represent a well-characterized unsteady regime with which to probe biomechanical responses of volant taxa to natural flow fluctuations.

In this regard, hummingbirds are of particular utility because of their capacity to engage in sustained feeding bouts from flowers over a range of orientations [11] and under challenging environmental conditions, including reduced air density [12], fast forward flight [13] and while flying in rain [14,15]. Thus, the associated maintenance of stability more generally is an obvious feature of flight in this taxon. Mask respirometry during flight is also a highly reliable method for hummingbirds [16], enabling direct measurement of the energetic consequences of different aerodynamic challenges.

We accordingly investigated the kinematic and metabolic responses of Anna's hummingbirds (*Calypte anna*) to flight within variably sized von Kármán vortex streets, and over a range of airspeeds. As with animal locomotion generally in spatially unpredictable environments (e.g. cockroach running [17], fish swimming [18]), we predicted an overall increase in kinematic variance and in the costs of flight relative to low-turbulence flow.

2. Material and methods

Five male Anna's hummingbirds were trapped, maintained in captivity for up to four weeks for experiments, and were then released into the wild. Individual birds were trained for several days to fly within the working section ($45.5 \times 45.5 \times 91.5$ cm) of a horizontal wind tunnel (Model 404, Engineering Laboratory Design, Lake City, MN, USA) operated at either 3, 6 or 9 m s^{-1} . Birds either perched or flew volitionally within the tunnel, and routinely fed from a horizontally oriented syringe (12 ml) filled with a commercial diet for nectar-feeding birds (Nektar-Plus, Nekton, Pforzheim, Germany). We placed cylinders (with diameters of either 2, 4 or 9 cm, and a height of 45 cm) vertically at the front of the tunnel's working section such that the feeding tip of the syringe was positioned downstream approximately 15 cm from the central axis of the cylinder (figure 1). The vertical position of the syringe within the working section was approximately 20 cm from the ceiling. Kinematic and metabolic measurements were made on each bird flying under 12 different experimental conditions (three airspeeds \times four treatments, with the latter corresponding to the three cylinder sizes and to one control treatment with no cylinder present).

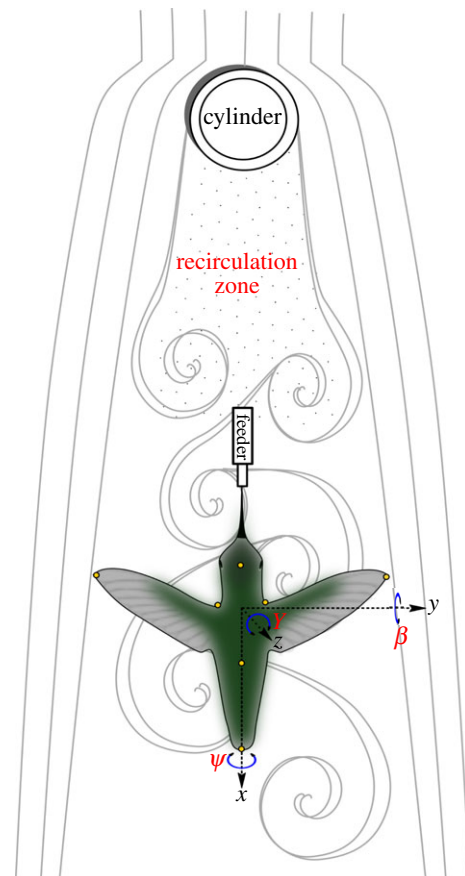


Figure 1. Top view of the experimental set-up used to study effects of von Kármán vortex streets on Anna's hummingbirds in forward flight. (Online version in colour.)

(a) Kinematic analysis

Hummingbirds feeding in flight from the syringe were filmed using two synchronized high-speed ($500 \text{ frames s}^{-1}$) video cameras (X-PRI, AOS Technologies AG, Switzerland) positioned laterally to and above the feeding syringe. We digitized positions of the top of the head, the shoulder tips, wing tips, tail root and tail tips in each video frame over eight flapping cycles, and translated these points to a three-dimensional coordinate system (x, y, z , with z aligned to gravity) using a direct linear transformation (DLT) [19]. Body points that were not visible from the right lateral camera view (i.e. the left wing tip and shoulder) were estimated and entered manually using lines projected from the DLT. Pitch angles of the body and tail were calculated using a projection onto the (x, z) plane of the vector formed by the head-back axis and the back-tail tip axis, respectively. Similarly, yaw angles of the body and tail were calculated using an orthogonal projection of the same vectors on the (x, y) plane. The orthogonal projection onto the (y, z) plane of the vector formed by the left to right shoulder axis was used to calculate roll. We tested whether cylinder treatments increased flight kinematic variance by evaluating standard deviations of mean variables, including γ_b (yaw of the body), γ_t (yaw of the tail), β_b (pitch of the body), β_t (pitch of the tail), ψ (roll of the body) and Φ (wingbeat amplitude for each wing), as well as n (wingbeat frequency for each wing). Maximal angles of body pitch, yaw and roll, as well as of tail pitch and yaw, were also determined over eight wingbeat cycles, and these are reported in the electronic supplementary material, table S1. We also measured the frequency of body yaw oscillations over eight wingbeat cycles (f_{yb}) to compare with estimated vortex shedding frequency (f_v) produced by the medium-sized and large cylinders. Values of f_{yb} were not measured for flight behind the small cylinder, because no discernible oscillation in yaw was evident for this treatment.

(b) Metabolic measurements

Oxygen uptake rates were measured for all treatments except for flight behind the small cylinder, for which preliminary data indicated no differences from the control treatment. Also, oxygen uptake could not be reliably measured for flight at 9 m s^{-1} within the wake of the large cylinder because birds could not continuously feed (i.e. for periods more than 2 s [20]) under this condition. Metabolic rates were determined using a respirometry mask [21] made from a 20 ml syringe cut to one-third of its length and positioned horizontally. One side of the mask was connected to the tip of a 10 ml syringe filled with nectar, such that the birds had to insert their entire head into the mask to feed. At the bottom of the respirometry mask, a tube (inner diameter: 4 mm) was connected to an airpump (Air Cadet 420–1901, Barnant, Barrington, IL, USA) via two 1 l containers. Air was sub-sampled from this latter tube using a FoxBox (Sable Systems International, Las Vegas, NV, USA), following scrubbing of water vapour using Drierite (W. A. Hammond, Xenia, OH, USA). Airflow was measured using a flowmeter (32446-33, Cole-Parmer, Vernon Hills, IL, USA) calibrated with a mass-flow calibrator (1E4-VCR-V-Q, DH Instruments Inc., Phoenix, AZ, USA). Mask airflow during all experiments averaged 4.11 l min^{-1} . The total oxygen consumed in a feeding bout was calculated by integrating the curve of oxygen over time from the initiation of feeding to the return to atmospheric level as described in [22] using the program EXPEDATA (Sable Systems International, Las Vegas, NV, USA), and following published equations [20,21]. The total volume of oxygen consumed during a feeding bout was divided by the total feeding time within the mask, as recorded via EXPEDATA using a photoresistor/LED pair attached to the feeder's opening and monitored electronically via the FoxBox [20]. The respiratory exchange ratio was assumed to be one [23]. We excluded metabolic data for which the feeding duration within the mask was too short for reliable measurement (i.e. less than 2 s [19]). Mass-specific metabolic rates were calculated using the mean of each bird's body mass as measured before and after daily experiments.

Respirometry measurements were validated by the argon dilution method [21] at the different experimental airspeeds and treatments using the following procedure. The extent of airflow dilution was measured six times at each combination of airspeed and treatment, and we then used one-way ANOVAs for airspeeds of 3 and 6 m s^{-1} to evaluate differences among treatments (i.e. the control, medium cylinder and large cylinder). For the airspeed of 9 m s^{-1} , we applied a *t*-test comparing the control with the medium cylinder treatment. There were no significant between-treatment differences at airspeeds of either 3 m s^{-1} ($F_{2,15} = 1.56$, $p = 0.24$) or 9 m s^{-1} ($t = 0.8$, d.f. = 8.2, $p = 0.45$). However, dilution associated with the large cylinder was significantly lower than the control at an airspeed of 6 m s^{-1} , by 5.4% on average ($F_{2,15} = 3.95$, $p = 0.04$; Tukey post-hoc test: $p = 0.03$). To incorporate this bias, we increased by this factor the estimated rates of oxygen uptake for hummingbirds flying at 6 m s^{-1} when the birds were in the wake of the large cylinder.

(c) Flow visualization

We used a smoke-wire technique [24] to visualize the wake produced by the three cylinder sizes at each tested airspeed. Airflow patterns were filmed from above at $500 \text{ frames s}^{-1}$, and associated digital videos were used to calculate the vortex shedding frequency (f_v) as averaged over five cycles. The Strouhal number for each treatment was calculated as $f_v L U^{-1}$, where f_v is the vortex shedding frequency, L is the cylinder diameter and U is the test airspeed. Values of the *Re* for each vortex shedding condition were also calculated as LUv^{-1} , where v is the kinematic viscosity of air ($1.46 \times 10^{-5} \text{ m}^2 \text{ s}^{-1}$).

We additionally used particle image velocimetry (PIV) to study the wake generated by the different cylinders over the experimental range of airspeeds. We seeded the wind tunnel with a cloud of olive oil microparticles generated with a LAVISION vaporizer (approx. $1 \mu\text{m}$ in diameter with a production rate of 1.4×10^{10} particles per second), and illuminated a horizontal sheet (approx. 2 mm thick) parallel to the floor of the wind tunnel using a double-pulsed 50 mJ Nd:Yag laser with a 15 Hz repetition rate (532 nm, Solo PIV, New Wave Research, ESI, Portland, OR, USA). An Image ProX CCD (1600×1200 pixels) camera was used to capture image pairs (separated by a time lag of $dt = 100 \mu\text{s}$) over an area of approximately $20 \times 26 \text{ cm}^2$. The camera was equipped with a 50 mm *f*/1.8 D Nikon lens, with the aperture set at 1.8. We used LaVision DAVIS software (v. 7.2.1.76) with a multipass correlation (128×128 and 32×32 , 50% overlap) to process the images into particle displacement measurements. During this processing, spurious vectors were removed by filtering on relative height of correlation peak (filter strength set at $Q < 1.3$), and by discarding vectors greater than twice the neighbouring RMS. The resulting vector fields were then smoothed with a local median average (3×3 window size). We also recorded PIV data for one hummingbird flying behind the cylinders, mainly to observe the position of the bird in relation to the vortex wake. At each airspeed and experimental treatment (i.e. three cylinders and the control condition), we recorded, at 15 Hz, five sequences each of 50 frames in duration. From these sequences, images were chosen that clearly showed shed vortices; these images were used to measure the wake length (λ). For the large cylinder, the wake length exceeded the dimensions of the working section and thus could not be estimated.

(d) Statistics

We applied repeated measures ANOVA, followed by a Tukey post-hoc test, at each of the three airspeeds to compare standard deviations among treatments for the rate of oxygen uptake and for the following kinematic variables: γ_b , γ_v , β_b , β_v , ψ , n and Φ . For metabolic rates measured at 9 m s^{-1} , we used a paired *t*-test to compare the control with the medium cylinder treatment. To fulfil the criteria of homogeneity of variance and normality in ANOVAs, we transformed the following variables: values at 3 m s^{-1} of γ_b , β_v , ψ and Φ (for both wings) were raised to fractional exponents; the logarithmic function was used for values of γ_b , γ_v , β_b , β_v , ψ and n at 6 m s^{-1} , and also for γ_b , γ_v , ψ and n at 9 m s^{-1} . Also at 9 m s^{-1} , values of Φ (for both wings) were raised to a fractional exponent. Similarly, values for metabolic rates were transformed at each of the three airspeeds using the multiplicative logarithm inverse. We tested for sphericity using Mauchly tests. In order to determine whether body oscillation frequencies (f_{yb}) and vortex shedding frequencies (f_v) were comparable at each airspeed, we performed unpaired *t*-tests. All statistical analyses were performed in R (v. 2.15.2) [25]. Data are presented as mean values ± 1 s.d. unless otherwise indicated.

3. Results

Wingbeat frequency increased with both cylinder size and airspeed (3 m s^{-1} : $n_{\text{left}}, F_{3,12} = 4.98$, $p = 0.017$; $n_{\text{right}}, F_{3,12} = 4.95$, $p = 0.018$; 6 m s^{-1} : $n_{\text{left}}, F_{3,12} = 4.63$, $p = 0.022$; $n_{\text{right}}, F_{3,12} = 4.02$, $p = 0.034$; 9 m s^{-1} : $n_{\text{left}}, F_{3,12} = 12.11$, $p < 0.001$; $n_{\text{right}}, F_{3,12} = 6.65$, $p < 0.001$), yet overall the increase with cylinder size was rather modest (approx. 10%; electronic supplementary material, table S2). Concurrently, the standard deviation in wingbeat frequency increased for flight behind medium and larger cylinders, but only at the two higher airspeeds (3 m s^{-1} : $n_{\text{left}}, F_{3,12} = 1.43$, $p = 0.28$; $n_{\text{right}}, F_{3,12} = 1.12$,

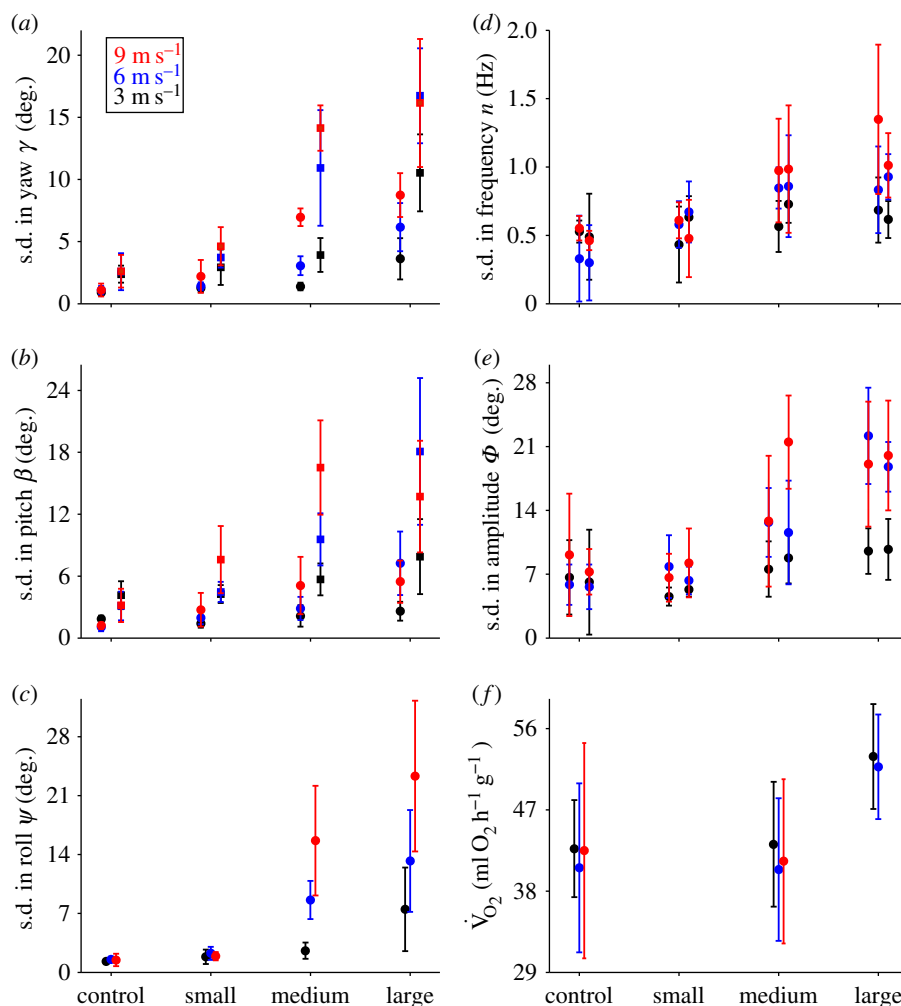


Figure 2. Variation in body and wingbeat kinematics, and values for metabolic rates and aerodynamic parameters of Anna's hummingbirds flying in the wake of von Kármán vortex streets generated by three cylinders of different diameters (2 cm, small; 4 cm, medium; 9 cm, large), and in an undisturbed control airflow, at airspeeds of 3 m s^{-1} (black), 6 m s^{-1} (blue) and 9 m s^{-1} (red): (a) average standard deviation of body yaw γ_b (circles) and tail yaw γ_t (squares); (b) average standard deviation of body pitch β_b (circles) and tail pitch β_t (squares); (c) average standard deviation of body roll ψ ; (d) average standard deviation of wingbeat frequency n (left circles: left wing, right circles: right wing); (e) average standard deviation of wingbeat amplitude for each wing Φ (left circles: left wing, right circles: right wing); (f) average values for mass-specific rates of oxygen uptake. For details, see text and table 1. Error bars indicate 1 s.d.

$p = 0.38$; 6 m s^{-1} : $n_{\text{left}} F_{3,12} = 4.64$, $p = 0.02$; $n_{\text{right}} F_{3,12} = 4.36$, $p = 0.027$; 9 m s^{-1} : $n_{\text{left}} F_{3,12} = 5.66$, $p = 0.01$; $n_{\text{right}} F_{3,12} = 4.95$, $p = 0.02$; figure 2d and table 1; also see the electronic supplementary material, tables S2–S4). Wingbeat amplitude overall decreased with airspeed but was not different among treatments (3 m s^{-1} : $\Phi_{\text{left}} F_{3,12} = 1.84$, $p = 0.19$; $\Phi_{\text{right}} F_{3,12} = 1.83$, $p = 0.20$; 6 m s^{-1} : $\Phi_{\text{left}} F_{3,12} = 0.66$, $p = 0.59$; $\Phi_{\text{right}} F_{3,12} = 0.25$, $p = 0.87$; 9 m s^{-1} : $\Phi_{\text{left}} F_{3,12} = 0.59$, $p = 0.66$; $\Phi_{\text{right}} F_{3,12} = 0.23$, $p = 0.87$; electronic supplementary material, table S2). By contrast, standard deviations in wingbeat amplitude for the two wings increased substantially with increasing cylinder size and airspeed (3 m s^{-1} : $\Phi_{\text{left}} F_{3,12} = 8.57$, $p = 0.002$; $\Phi_{\text{right}} F_{3,12} = 4.01$, $p = 0.034$; 6 m s^{-1} : $\Phi_{\text{left}} F_{3,12} = 12.33$, $p < 0.001$; $\Phi_{\text{right}} F_{3,12} = 13.43$, $p < 0.001$; 9 m s^{-1} : $\Phi_{\text{left}} F_{3,12} = 4.11$, $p = 0.031$; $\Phi_{\text{right}} F_{3,12} = 12.11$, $p < 0.001$; figure 2e and table 1).

Mass-specific metabolic rate varied significantly with treatment at 3 m s^{-1} ($F_{2,8} = 10.2$, $p = 0.006$) and at 6 m s^{-1} ($F_{2,8} = 5.7$, $p = 0.03$), but not at 9 m s^{-1} ($t = 0.7$, d.f. = 4, $p = 0.6$; note that metabolic rates could not be measured for the large cylinder treatment at this airspeed). Metabolic rates were significantly higher for flight behind the large cylinder at 3 m s^{-1} compared with both the control (Tukey

post-hoc comparison, $Z = 3.95$, $p = 0.0002$) and the medium-sized cylinder ($Z = 3.88$, $p = 0.0003$), and the same effect was found for flight at 6 m s^{-1} when compared with the control ($Z = 3.18$, $p = 0.004$) and with the medium cylinder ($Z = 2.60$, $p = 0.025$) treatments. Metabolic rates were not significantly different between the control and medium cylinder treatments at 3 m s^{-1} ($Z = -0.065$, $p = 1$), 6 m s^{-1} ($Z = -0.57$, $p = 0.83$) and 9 m s^{-1} (see above). Hummingbird flight metabolic rate increased by about 25% when flying in the wake of the large cylinder at both 3 m s^{-1} and 6 m s^{-1} (figure 2f).

The standard deviation of body yaw (γ_b) increased significantly with increasing cylinder size at 3 m s^{-1} ($F_{3,12} = 11.6$, $p < 0.001$), 6 m s^{-1} ($F_{3,12} = 33.3$, $p < 0.001$) and 9 m s^{-1} ($F_{3,12} = 39.1$, $p < 0.001$; see also table 1; electronic supplementary material, table S1–S4). The standard deviation of tail yaw (γ_t) varied similarly but to a greater extent, specifically for flight in the wakes of the medium and large cylinders at both 6 m s^{-1} and 9 m s^{-1} (figure 2a and table 1; 3 m s^{-1} : $F_{3,12} = 18.81$, $p < 0.001$; 6 m s^{-1} : $F_{3,12} = 38.5$, $p < 0.001$; 9 m s^{-1} : $F_{3,12} = 32.8$, $p < 0.001$). Standard deviation of body pitch (β_b) did not vary with treatment at 3 m s^{-1} ($F_{3,12} = 2.6$, $p = 0.1$), but increased

Table 1. Standard deviations in kinematic variables (γ_{bv} , γ_{lv} , β_{bv} , β_{lv} , ψ_l , n_{right} , n_{left} , Φ_{right} and Φ_{left}) for Anna's hummingbirds, the mass-specific metabolic rate, and vortex shedding parameters at different airspeeds and for three experimental treatments and control conditions ($n = 5$ birds in all cases except for St and Re). See text for definitions and details. Kinematic values correspond to the mean standard deviation ± 1 s.d. and mass-specific metabolic rate corresponds to the mean value ± 1 s.d. Different superscript letters represent statistically different groups following post-hoc tests, for which details are given in the electronic supplementary material, table S2.

treatment	γ_{lv} (deg.)	γ_{bv} (deg.)	β_{lv} (deg.)	β_{bv} (deg.)	ψ_l (deg.)	Φ_{right} (deg.)	Φ_{left} (deg.)	n_{right} (Hz)	n_{left} (Hz)	\dot{V}_{O_2} (ml O ₂ h ⁻¹ g ⁻¹)	St	Re ($\times 10^3$)	f_r (Hz)	f_{vb} (Hz)
3 m s ⁻¹														
control	2.4 \pm 0.7 ^a	0.9 \pm 0.2 ^a	4.2 \pm 1.4 ^a	1.8 \pm 0.3 ^a	1.3 \pm 0.3 ^a	6.1 \pm 5.8 ^a	6.7 \pm 4.1 ^a	0.5 \pm 0.3 ^a	0.5 \pm 0.1 ^a	42.7 \pm 5.4 ^a	—	—	—	—
small	2.9 \pm 1.4 ^a	1.3 \pm 0.3 ^a	4.3 \pm 0.9 ^a	1.4 \pm 0.4 ^a	1.9 \pm 0.9 ^{ab}	5.3 \pm 0.8 ^{ab}	4.5 \pm 1.0 ^a	0.6 \pm 0.2 ^a	0.4 \pm 0.3 ^a	—	0.2	4.1	29.5 \pm 1.2	—
medium	3.9 \pm 1.4 ^b	1.4 \pm 0.3 ^a	5.7 \pm 1.5 ^a	2.1 \pm 1.0 ^b	2.6 \pm 1.0 ^b	8.8 \pm 2.8 ^{ab}	7.6 \pm 3.0 ^a	0.7 \pm 0.1 ^a	0.6 \pm 0.2 ^a	43.2 \pm 6.9 ^a	0.24	8.2	17.8 \pm 0.8	12.3 \pm 4.7
large	10.5 \pm 3.1 ^b	3.6 \pm 1.7 ^b	7.9 \pm 3.6 ^a	2.6 \pm 0.9 ^a	7.5 \pm 5.0 ^c	9.7 \pm 3.3 ^{ac}	9.5 \pm 2.5 ^a	0.6 \pm 0.1 ^a	0.7 \pm 0.2 ^a	52.9 \pm 5.8 ^b	0.22	18.5	7.5 \pm 0.3	7.8 \pm 0.8
6 m s ⁻¹														
control	2.6 \pm 1.5 ^a	1.1 \pm 0.3 ^a	3.1 \pm 1.4 ^a	1.1 \pm 0.4 ^a	1.5 \pm 0.3 ^a	5.6 \pm 2.4 ^a	5.9 \pm 2.2 ^a	0.3 \pm 0.3 ^a	0.3 \pm 0.3 ^a	40.6 \pm 9.4 ^a	—	—	—	—
small	3.7 \pm 0.8 ^a	1.4 \pm 0.3 ^a	4.5 \pm 1.0 ^a	2 \pm 0.6 ^b	2.3 \pm 0.8 ^a	6.3 \pm 1.5 ^{ab}	7.8 \pm 3.4 ^a	0.7 \pm 0.2 ^{ab}	0.6 \pm 0.2 ^{ab}	—	0.2	8.2	59.7 \pm 3.8	—
medium	10.9 \pm 4.7 ^b	3.1 \pm 0.8 ^b	9.6 \pm 2.5 ^b	2.9 \pm 1.1 ^b	8.6 \pm 2.3 ^b	11.6 \pm 5.7 ^b	12.7 \pm 3.8 ^b	0.9 \pm 0.4 ^b	0.8 \pm 0.2 ^b	40.4 \pm 7.9 ^b	0.22	16.4	33 \pm 1.9	12.3 \pm 2.9
large	16.7 \pm 3.8 ^b	6.2 \pm 1.9 ^c	18.1 \pm 7.1 ^c	7.2 \pm 3.1 ^c	13.2 \pm 6.0 ^b	18.8 \pm 2.7 ^c	22.2 \pm 5.3 ^c	0.9 \pm 0.2 ^b	0.8 \pm 0.3 ^b	51.8 \pm 5.8 ^b	0.25	37.0	16.9 \pm 0.8	19 \pm 2.8
9 m s ⁻¹														
control	2.6 \pm 1.3 ^a	1.1 \pm 0.5 ^a	3.2 \pm 1.6 ^a	1.2 \pm 0.3 ^a	1.5 \pm 0.7 ^a	7.3 \pm 2.5 ^a	9.1 \pm 6.7 ^a	0.5 \pm 0.1 ^a	0.6 \pm 0.1 ^a	42.5 \pm 11.9 ^a	—	—	—	—
small	4.6 \pm 1.5 ^b	2.2 \pm 1.3 ^b	7.6 \pm 3.3 ^{ab}	2.7 \pm 1.6 ^{ab}	1.9 \pm 0.5 ^a	8.2 \pm 3.8 ^a	6.6 \pm 2.6 ^a	0.5 \pm 0.3 ^a	0.6 \pm 0.1 ^{ab}	—	0.19	12.3	84.3 \pm 10.2	—
medium	14.1 \pm 1.8 ^c	7 \pm 0.7 ^c	16.5 \pm 4.6 ^c	5.1 \pm 2.8 ^b	15.7 \pm 6.5 ^b	21.5 \pm 5.1 ^b	12.8 \pm 7.2 ^{ab}	1.0 \pm 0.5 ^b	1.0 \pm 0.4 ^{bc}	41.3 \pm 9.1 ^a	0.23	24.7	52.7 \pm 6.5	11.4 \pm 2.9
large	16.2 \pm 5.2 ^c	8.7 \pm 1.8 ^c	13.7 \pm 5.4 ^{bc}	5.5 \pm 2.1 ^b	23.3 \pm 9.0 ^b	20 \pm 6.0 ^b	19.1 \pm 6.9 ^b	1.0 \pm 0.2 ^b	1.3 \pm 0.5 ^c	—	0.25	55.5	24.6 \pm 1.4	22.1 \pm 2.3

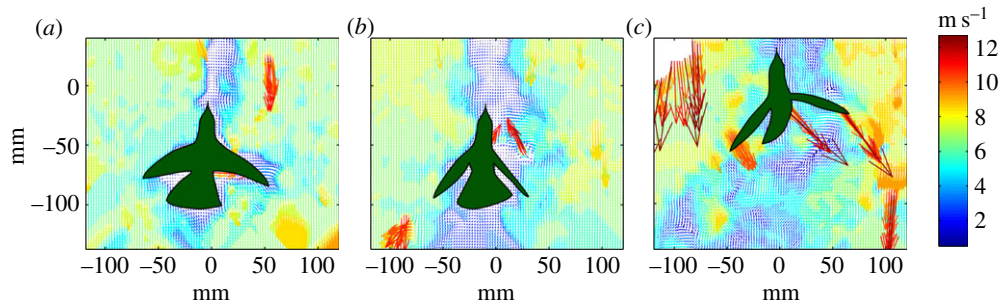


Figure 3. PIV-derived velocity fields images for an Anna's hummingbird flying in the vortex street for the (a) small, (b) medium and (c) large cylinders, at a free-stream velocity of 6 m s^{-1} .

significantly at higher airspeeds (6 m s^{-1} : $F_{3,12} = 23.3$, $p < 0.001$; 9 m s^{-1} : $F_{3,12} = 5.8$, $p = 0.01$), and to a substantial extent for flight in the wakes of the medium and large cylinders at 6 m s^{-1} ($F_{3,12} = 23.3$, $p < 0.001$) and 9 m s^{-1} ($F_{3,12} = 5.8$, $p = 0.01$), compared with their respective controls. The same trend was found for standard deviations in tail pitch (β_t), and also only at 6 and 9 m s^{-1} for the medium and large cylinders compared with controls (3 m s^{-1} : $F_{3,12} = 2.9$, $p = 0.08$; 6 m s^{-1} : $F_{3,12} = 26.4$, $p < 0.001$, and 9 m s^{-1} : $F_{3,12} = 10.6$, $p = 0.0011$). This effect was overall greater for the standard deviations in tail pitch, especially at high airspeeds (figure 2*b*). Standard deviation for body roll was significantly higher for flights within the wake of the medium and large cylinders (3 m s^{-1} : $F_{3,12} = 11.0$, $p < 0.001$; 6 m s^{-1} : $F_{3,12} = 60.1$, $p < 0.001$, and 9 m s^{-1} : $F_{3,12} = 43.3$, $p < 0.001$; figure 2*c*), with steeply increasing maximal body rolls of up to 45° (electronic supplementary material, tables S2–S4).

Yaw oscillation frequencies f_{yb} did not differ significantly from vortex shedding frequencies f_v at any airspeed for the large cylinder treatment (3 m s^{-1} : unpaired t -test, $t = 0.7$, d.f. = 8, $p = 0.48$; 6 m s^{-1} : $t = 1.6$, d.f. = 8, $p = 0.15$; 9 m s^{-1} : $t = -2.1$, d.f. = 8, $p = 0.07$). However, f_{yb} in the medium cylinder treatment was significantly smaller than f_v for flight at 3 m s^{-1} (unpaired t -test, $t = -2.6$, d.f. = 8, $p = 0.003$), 6 m s^{-1} ($t = -13.4$, d.f. = 8, $p < 0.001$) and 9 m s^{-1} ($t = -12.9$, d.f. = 8, $p < 0.001$; table 1). Wake lengths for the small cylinder at 3 , 6 and 9 m s^{-1} were 10.15 ± 0.66 , 10.20 ± 0.82 and 10.75 ± 0.92 cm, respectively (values correspond to the mean ± 1 s.d.). For the medium cylinder, wake lengths averaged 16.90 ± 1.77 , 17.30 ± 0.85 and 16.70 ± 1.04 cm, respectively. Figure 3 illustrates the position of a hummingbird within the three different cylinder wakes at an airspeed of 6 m s^{-1} . Overall, hummingbirds flying within von Kármán vortex streets employed asymmetric tail and wing motions for compensation while maintaining a highly stabilized head posture to enable aerial feeding. Such tail and wing corrections, including intermittent differences in amplitude between the wings, are clearly visible when birds flew at 6 m s^{-1} and 9 m s^{-1} within the large cylinder's wake (figure 4; electronic supplementary material SV2–SV4).

4. Discussion

During their daily routines, free-ranging aerial taxa can be challenged by a broad spectrum of unsteady airflows, including vortex wakes shed by vegetation, convective thermals,

turbulent wind shear and even spontaneous whirlwinds. Here, we have shown that hummingbird flight metabolic rates and kinematics can be markedly affected by relatively large vortex wakes, which impose an impressive increase in the costs of flight (e.g. by 25% for flight in the wake of the large cylinder; figure 2*f*). Maintenance of stability, via leg extension (as in orchid bees [4]) or via wing and tail readjustment as shown here for hummingbirds (figures 2*a–c* and 4) will be scale-dependent given the damping effects of large body size on rotational accelerations [26]. For hummingbirds (and members of the Apodidae more generally), diminutive feet and legs preclude use of these structures to enhance the inertial resistance to roll, although short legs are likely to enhance balance while perching for small birds [27].

To effect stable flight under the experimental conditions studied here, hummingbirds must primarily overcome yaw and roll torques induced by shed vortices. Animal gliders and airplanes can perform symmetrically banked turns to reorient laterally the vertical force vector and thus to yaw [28]. Hummingbirds can also perform pure yaw turns while flapping their wings either symmetrically [29] or asymmetrically [30,31]. We did not quantitatively analyse body, wing and tail asymmetries in relation to the temporal sequence of variable fluid motions, but a diversity of kinematic responses (including rolls, tail deformations, body flexion and bilateral wing geometries) are qualitatively evident when the birds fly within the most extreme vortex wake (figure 4 and electronic supplementary material, video S4). Although mean wingbeat amplitude was unaltered among cylinder treatments and control (electronic supplementary material table S1), and mean wingbeat frequency changed only somewhat with cylinder size, standard deviations in both variables increased dramatically with cylinder size relative to controls, by values as high as 200% and 50%, respectively (table 1). These responses, in aggregate, reflect changes both in wake unsteadiness and in the velocity deficit (electronic supplementary material, table S5), particularly for the large cylinder. Even at speeds of 9 m s^{-1} under these conditions, however, hummingbirds exhibit maximal body and tail yaw amplitudes near 30° and 60° , respectively. By contrast, hawkmoths flying into large vortices (i.e. those produced with a cylinder diameter comparable to the wing span) exhibit average yaw amplitudes near 60° at low flight speeds of only 2 m s^{-1} [32]. This comparison suggests that tail displacements play a major role in damping yaw oscillations induced on hummingbirds. Analogous adjustment in body and tail postures, along with changes in wingbeat kinematics, enable hummingbirds to maintain stable flight in heavy rain [14,15]. Use of tail motions in flight control has also

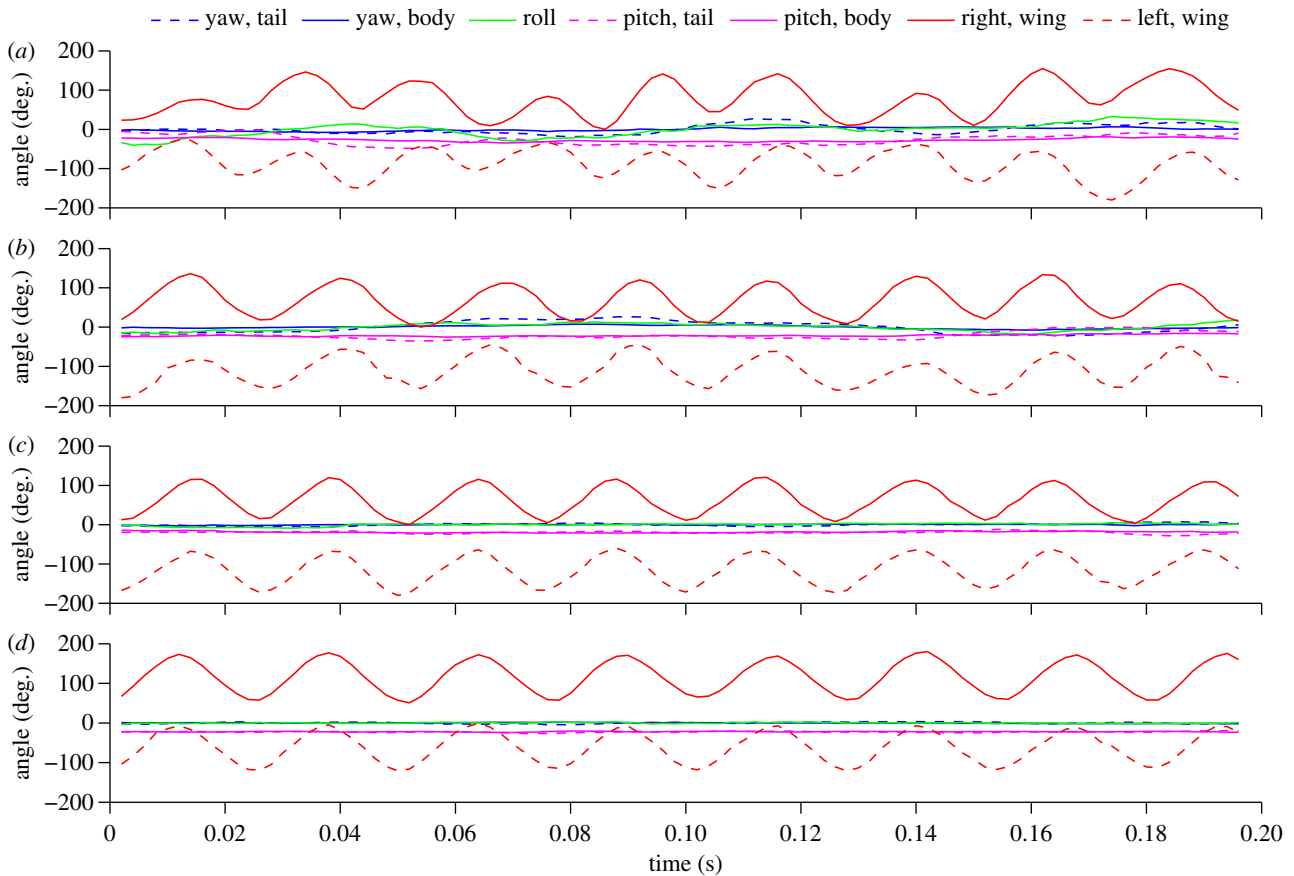


Figure 4. Time series for the wing, body and tail angles of a hummingbird flying at 6 m s^{-1} behind a (a) large, (b) medium and (c) small cylinder, and in an unperturbed control flow (d). The blue lines represent body yaw (solid line) and tail (dashed line), respectively; the pink lines represent body pitch (solid line) and tail pitch (dashed line), respectively; the green line represents body roll; red lines represent right (solid line) and left (dashed line) wing positions, respectively. See text for details.)

been recently demonstrated for the Japanese white-eye (*Zosterops japonicus*). During slow flight, this passerine regulates body posture by cyclically changing the pitch and the spreading of the tail, in synchronization with wing motions [33]. Similarly, hummingbirds may use their tails within the induced flow field of the wings to regulate body pitch [34]. When in the vortex wakes described here, flying hummingbirds may use tail spreading to avoid extreme sideslip, roll and pitching on very short timescales (electronic supplementary material SV1–SV3).

For swimming fish, various issues of control, muscle activation and metabolic performance arise in perturbed flows [6,7]. Stability challenges have been identified, for example, when the diameter of the largest vortices in the flow approaches the fish's body length [35], resulting in a loss of postural control and reduction of swimming speed. Unlike fish, however, hover-feeding hummingbirds are forced to maintain tight millimetre-level positioning of the hummingbird head during flight. Head mobility relative to the body is, however, very high, given that the hummingbird head can be rotated more than 180° in less than 2 ms [15]. We did notice matching between body oscillations and vortex shedding frequencies for flight behind the large cylinder (table 1), although this effect was not seen for the much higher shedding frequencies produced by the small and medium cylinders. Given the high variability seen in wingbeat and tail kinematics at different airspeeds and with different cylinder sizes, a diversity of compensatory mechanisms may be at play in such flights. At least

for flight in large eddies, these are associated with a substantial increase in the metabolic cost of flight (figure 2f). Because of the ratio of the large cylinder's diameter relative to the wing span (e.g. approx. 0.75), associated eddies must interact not just with the body or a single wing but with the entire wing disc, challenging the ability of the birds to correct for perturbations. Eddies behind the small and medium cylinders will be much smaller (given cylinder diameter: wingspan ratios of 0.17 and 0.33, respectively) and induce no metabolic changes relative to the control (figure 3). Analogous findings [35] for fish suggest that this may represent a generalization of the size-dependent effects of flow perturbation on animal locomotion.

Our study suggests that the length scale of turbulent vortex shedding is an important factor that influences compensatory mechanisms. Shed vortices smaller than a wing length have minimal effects on flight kinematics even at higher speeds, whereas those sized similar to or greater than the wing length induce greater variance in wing and body kinematics, particularly at higher speeds. Individuals flying in wakes behind the small and medium cylinders will also pass through multiple vortices such that torque induced by an initial vortex will in part be compensated by a second incoming vortex of opposite rotational sense. Meanwhile, hummingbirds flying behind the large cylinder will encounter only one vortex at a time, and may thus need to disproportionately change body and tail kinematics to compensate for changes in streamwise and transverse velocities downstream of the large cylinder (electronic supplementary

material, figure S2). Similar results would also be seen in the more complex flow found in natural canopies, because large turbulent motions will affect birds far more than small ones. This suggests that the spatial energy spectrum of environmental turbulence is worth measuring, not simply the velocity variance magnitude which is often reported as ‘turbulence intensity’. Moreover, turbulence can potentially limit maximum flight speeds (e.g. [4]). It was not possible for hummingbirds to fly and feed stably in wakes of the large cylinder produced at stream velocities of 12 m s^{-1} , although in unperturbed flow they can fly as fast as 14 m s^{-1} [13]. Similarly, hawkmoths reach a maximal speed of 2 m s^{-1} while flying in large vortices, but well exceed this value in laminar flow, flying at 3 m s^{-1} [32].

Vortex shedding by a circular cylinder is characterized by a recirculation region and a periodic wake characterized by fluctuations in the streamwise and spanwise directions (and only weak vertical velocity variance) [5]. The interplay between the recirculation and the wake is complex, leading to a sequence of different dynamical regimes observed with increasing Re [5]. All of the cases studied here fall into a single regime, which is denoted the D-E regime and described in detail by Williamson [5]. Our measurements of the non-dimensional shedding frequency (St ; table 1) agree with those expected for our values of Re [5], and vortex shedding measurements can more generally be used to predict both the size of the recirculation region and the velocity variance in the wake region as a function of distance downstream. Wake velocity fluctuations in both lateral and streamwise planes are inversely correlated with the normalized distance downstream, $r_{x/D}$ (i.e. the ratio of the downstream distance to cylinder diameter). At Re between 10^3 and 10^4 , these velocity fluctuations show high variation in the recirculation region (i.e. $r_{x/D} < 3$), moderate variation at $3 < r_{x/D} < 5$ and decay when $r_{x/D} > 5$ [36]. In this study, values of $r_{x/D}$ for the large, medium and small cylinders (using the central axis of the cylinder as the origin) were 2, 4 and 8, respectively, indicating that hummingbirds in the wake of the large cylinder are exposed to substantial recirculating flows.

Experimental and computational studies of wakes produced by circular cylinders at Reynolds numbers near 1000 also indicate that the normalized variance of streamwise speed compared with the unsteady flow speed over the cylinder centreline is approximately 8% at $r_{x/D} = 2$ and approximately 4% at $r_{x/D} = 8$ [36]. Concomitantly, the normalized variance in transverse speed is up to approximately 50% at $r_{x/D} = 2$ and approximately 20% at $r_{x/D} = 8$ [36]. Here, PIV measurements of the wake velocity field at the feeder location for the small, medium and large cylinders, respectively, indicate that average horizontal velocities were 20, 20 and 40% lower than the free-stream velocity at 3 m s^{-1} ; 10, 10 and 30% lower at 6 m s^{-1} , respectively; and 10, 10 and 20% at 9 m s^{-1} , respectively (electronic supplementary material, table S5). Thus, changes in wake velocities produced at the feeder position and at each speed were fairly similar between the small and medium cylinders, but the wake for the large cylinder speeds exhibited a much greater relative reduction compared with free-stream velocity (electronic supplementary material, table S5 and figure S2). We thus predict greater variation in pitch, roll and yaw for this latter experimental condition, with more change in roll and yaw than in pitch given the predicted variance in transverse speeds relative to that of streamwise speeds. It is important to note that direct flow

comparisons among different cylinders are only appropriate if the regimes share the same Reynolds numbers. Here, the Reynolds number for the large cylinder was twice and fivefold higher than those for the medium and small cylinders, respectively (table 1). Experimentally, we used a fixed downstream distance as the reference point for study because a much wider range of airspeeds among treatments would have been necessary to effect Reynolds number equivalence, rendering kinematic performance and flight energetics more difficult to compare among cylinders. However, the reference point for each of the study cylinders used here was always within the near wake (i.e. $r_{x/D} < 10$) where the vortex street is still well-structured despite flow instabilities and decay (electronic supplementary material, video S4). Experimental evidence for moths also indicates that flight either in the recirculation zone or far downstream from a cylinder of one wing length in diameter produces similar responses [32].

For hummingbirds in the vortex sheets generated by the large cylinder, variation in pitch (for both the tail and body) exceeded that of the small cylinder by a factor of 2–4, for yaw (in both tail and body) by a factor of 3–5 and for roll by a factor of 4–12. Pitch variation is thus comparable to variation between these two cylinders in velocities (i.e. by a factor of two; electronic supplementary material, table S5), but variation in yaw and roll is substantially greater. By contrast, hummingbirds behind the small cylinder were flying in a region where velocity fluctuations are much lower, which should yield reduced consequences for flight kinematics and metabolic costs. It is important to note that at these flow regimes ($Re > 10^3$), the wake formed behind a cylinder becomes irregular with a St of approximately 0.21 (St measured here was 0.22; table 1) and is characterized by three-dimensional shedding instabilities and turbulence [37]. Here, this turbulent effect within the wake (electronic supplementary material, SV5; figure S1) may also have contributed to the high variation characterizing most kinematic variables. It is important to note that, in spite of these effects, birds maintained average values of roll and yaw very close to zero through flights, effectively avoiding a net skew relative to airflow (electronic supplementary material, table S6).

The power curve for male Anna’s Hummingbirds has been empirically determined using mask respirometry across the entire airspeed range for the species, from a fast 14 m s^{-1} down to hovering in still air [38], and also for backward flight [22]. As suggested by aerodynamic models [28] the power curve exhibited a minima at intermediate forward air speeds because of high induced drag during hovering and slow flight, and high parasite and profile drags during high-speed forward flight. At the airspeeds measured here (3, 6 and 9 m s^{-1}), net aerodynamic costs are significantly lower [38] relative to hovering or fast forward flight. As flight within vortices requires overcoming control challenges, at least for the large and medium cylinder size treatments (see the electronic supplementary material SV1–SV3), introducing flow perturbations at maximal or sub-maximal airspeeds would probably increase flight costs with concomitant kinematic changes, as suggested here from mask respirometry measurements at 9 m s^{-1} . Interestingly, we found no airspeed-related variation in flight metabolism; vortex size-related differences were, nonetheless, substantial. Flight metabolic rates were similar for all airspeeds at both the control and the medium cylinder treatments, whereas these were significantly elevated for the large cylinder treatment at both 3 m s^{-1} and 6 m s^{-1} . Although one

might expect an increasing effect with airspeed, as found for orchid bees flying within a highly turbulent flow [2], our findings suggest that vortex shedding may have important effects on flight metabolism even at low forward airspeeds (figure 2). Consequently, even mild environmental winds may impose increased energetic costs if associated vortices are in the size range of 0.75–1 wingspans.

Ecologically, airflow perturbations and wind regime may influence habitat selection during foraging for diverse aerial nectarivores, as well as, more generally, for animals engaged in various types of flights. For example, nocturnal migratory passerines expend more energy during flight when the atmosphere is turbulent [39]. Similarly, turbulence intensity influences fish habitat selection in streams [40,41]. The biomechanical consequences of such turbulence will depend on a variety of factors, as demonstrated here for vortex size in relation to animal dimensions, along with the speed of the fluid. Additional effects that occur in real-world environments will include vortex orientation and overall intensity of turbulence. Flow structures both deep inside and at the top of the canopy are dominated by von Kármán vortex streets and Kelvin–Helmholtz instabilities, respectively [10]. Common daily activities of hummingbirds, such as foraging (for nectar, arthropods or nest material), chases, landing and take-off will thus all be affected by turbulent flow. Also, turbulence in the canopy can be intermittent on longer timescales, making it hard for fliers to predict when and where turbulent flows will occur. Our experimental results suggest that strong and relatively large turbulence (when compared with body size) characteristic of natural

environments can induce compensatory kinematic responses that may substantially increase metabolic requirements of flight. Laboratory measurements of flight energetics in reduced or even negligibly turbulent experimental flows may thus not strictly be applicable to estimates of the costs of flight in the field. These costs may, nonetheless, contribute substantially to daily energetic expenditure for a wide range of flying taxa. The effects of relative size for the consequences of vortical flows, as described here, may be similarly relevant for birds, bats and volant hexapods of widely different sizes, with wingspans ranging from several millimetres to 3 m. Future work assessing metabolic consequences of turbulent flow regimes differing in structure and magnitude would also be informative.

This research was conducted in compliance with Animal Use Protocol #R282-0310 at the University of California, Berkeley. Live bird trapping was carried out under permits from the United States Fish and Wildlife Service (MB054440-0) and the California Department of Fish and Game (SC-006627).

Acknowledgements. We thank Sarahi Arriaga for her assistance with Matlab programming for the kinematic analysis, and members of the UC-Berkeley animal flight laboratory for technical assistance. V.M.O.-J., N.S., M.W., E.V. and R.D. designed research; V.M.O.-J., N.S., M.W. performed research; V.M.O.-J. and N.S. analysed data; and V.M.O.-J., N.S., M.W., E.V. and R.D. wrote the paper. The authors declare no conflict of interest.

Funding statement. This work was supported by AFOSR #13RSA030, the University of California MEXUS-CONACYT program, and the Swedish Research Council.

References

- Tucker VA. 1972 Metabolism during flight in the laughing gull, *Larus atricilla*. *Am. J. Physiol.* **222**, 237–245.
- Pennycuik CJ, Alerstam T, Hedenström A. 1997 A new low-turbulence wind tunnel for bird flight experiments at Lund University, Sweden. *J. Exp. Biol.* **200**, 1441–1449.
- Engel S, Bowlin MS, Hedenström A. 2010 The role of wind-tunnel studies in integrative research on migration biology. *Integr. Comp. Biol.* **50**, 323–335. (doi:10.1093/icb/icc063)
- Combes SA, Dudley R. 2009 Turbulence-driven instabilities limit insect flight performance. *Proc. Natl Acad. Sci. USA* **106**, 9105–9108. (doi:10.1073/pnas.0902186106)
- Williamson HK. 1996 Vortex dynamics in the cylinder wake. *Annu. Rev. Fluid Mech.* **28**, 477–539. (doi:10.1146/annurev.fl.28.010196.002401)
- Liao JC. 2007 A review of fish swimming mechanics and behaviour in altered flows. *Phil. Trans. R. Soc. B* **362**, 1973–1993. (doi:10.1098/rstb.2007.2082)
- Liao JC, Beal DN, Lauder GV, Triantafyllou M. 2003 Fish exploiting vortices decrease muscle activity. *Science* **302**, 1566–1569. (doi:10.1126/science.1088295)
- Beal DN, Hover FS, Triantafyllou MS, Liao JC, Lauder GV. 2006 Passive propulsion in vortex wakes. *J. Fluid Mech.* **549**, 385–402. (doi:10.1017/S0022112005007925)
- McCay MG. 2003 Winds under the rain forest canopy: the aerodynamic environment of gliding tree frogs. *Biotropica* **35**, 94–102. (doi:10.1111/j.1744-7429.2003.tb00266.x)
- Poggi D, Porporato A, Ridolfi L, Albertson JD, Katul GG. 2004 The effect of vegetation density on canopy sub-layer turbulence. *Boundary-Layer Meteorol.* **111**, 565–587. (doi:10.1007/s10546-009-9423-1)
- Sapir N, Dudley R. 2013 Implications of floral orientation for flight kinematics and metabolic expenditure of hover-feeding hummingbirds. *Funct. Ecol.* **27**, 227–235. (doi:10.1111/1365-2435.12024)
- Chai P, Dudley R. 1995 Limits to vertebrate locomotor energetics suggested by hummingbirds hovering in heliox. *Nature* **377**, 722–725. (doi:10.1038/377725a0)
- Clark CJ, Dudley R. 2009 Flight costs of long, sexually selected tails in hummingbirds. *Proc. R. Soc. B* **276**, 2109–2115. (doi:10.1098/rspb.2009.0090)
- Ortega-Jimenez VM, Dudley R. 2012 Flying in the rain: hovering performance of Anna's hummingbirds under varied precipitation. *Proc. R. Soc. B* **279**, 3996–4002. (doi:10.1098/rspb.2012.1285)
- Ortega-Jimenez VM, Dudley R. 2012 Aerial shaking performance of wet Anna's hummingbirds. *J. R. Soc. Interface* **9**, 1093–1099. (doi:10.1098/rsif.2011.0608)
- Welch KC. 2011 The power of feeder-mask respirometry as a method for examining hummingbird energetics. *Comp. Biochem. Physiol. A* **158**, 276–286. (doi:10.1016/j.cbpa.2010.07.014)
- Sponberg S, Full RJ. 2008 Neuromechanical response of musculo-skeletal structures in cockroaches during rapid running on rough terrain. *J. Exp. Biol.* **211**, 433–446. (doi:10.1242/jeb.012385)
- Enders EC, Boisclair D, Roy AG. 2003 The effect of turbulence on the cost of swimming for juvenile Atlantic salmon (*Salmo salar*). *Can. J. Fish Aquat. Sci.* **60**, 1149–1160. (doi:10.1139/f03-101)
- Hedrick TL. 2008 Software techniques for two- and three-dimensional kinematic measurements of biological and biomimetic systems. *Bioinspir. Biomim.* **3**, 034001. (doi:10.1088/1748-3182/3/3/034001)
- Bartholomew GA, Lighton JRB. 1986 Oxygen consumption during hover-feeding in free-ranging Anna's hummingbirds. *J. Exp. Biol.* **123**, 191–199.
- Lighton JRB. 2008 *Measuring metabolic rates - a manual for scientists*. New York, NY: Oxford University Press.
- Sapir N, Dudley R. 2012 Backward flight in hummingbirds employs unique kinematic

- adjustments and entails low metabolic cost. *J. Exp. Biol.* **215**, 3603–3611. (doi:10.1242/jeb.073114)
23. Welch Jr KC, Altshuler DL, Suarez RK. 2007 Oxygen consumption rates in hovering hummingbirds reflect substrate-dependent differences in P/O ratios: carbohydrate as a 'premium fuel'. *J. Exp. Biol.* **210**, 2146–2153. (doi:10.1242/jeb.005389)
24. Marzkirch W. 1987 *Flow visualization*, 2nd edn. London, UK: Academic Press.
25. R Development Core Team. 2012 *R: a language and environment for statistical computing*. Vienna, Austria: R Foundation for Statistical Computing. (<http://www.R-project.org>)
26. Dudley R. 2002 Mechanisms and implications of animal flight maneuverability. *Integr. Comp. Biol.* **42**, 135–140. (doi:10.1093/icb/42.1.135)
27. Schulenberg TS. 1983 Foraging behavior, ecomorphology, and systematics of some antshrikes (Formicariidae: Thamnomanes). *Wilson Bull.* **95**, 505–521.
28. Norberg UM. 1990 *Vertebrate flight: mechanics, physiology, morphology, ecology and evolution*. Berlin, Germany: Springer.
29. Hedrick TL, Cheng B, Deng X. 2009 Wingbeat time and the scaling of passive rotational damping in flapping flight. *Science* **324**, 252–255. (doi:10.1126/science.1168431)
30. Altshuler DL, Quicazán-Rubio EM, Segre PS, Middleton KM. 2012 Wingbeat kinematics and motor control of yaw turns in Anna's hummingbirds (*Calypte anna*). *J. Exp. Biol.* **215**, 4070–4084. (doi:10.1242/jeb.075044)
31. Fry SN, Sayaman R, Dickinson MH. 2003 The aerodynamics of free-flight maneuvers in *Drosophila*. *Science* **300**, 495–498. (doi:10.1126/science.1081944)
32. Ortega-Jimenez VM, Greeter JS, Mittal R, Hedrick TL. 2013 Hawkmoth flight stability in turbulent vortex streets. *J. Exp. Biol.* **216**, 4567–4579. (doi:10.1242/jeb.089672)
33. Su JY, Ting SC, Chang YH, Yang JT. 2012 A passerine spreads its tail to facilitate a rapid recovery of its body posture during hovering. *J. R. Soc. Interface* **9**, 1674–1684. (doi:10.1098/rsif.2011.0737)
34. Altshuler DL, Princevac M, Pan H, Lozano J. 2009 Wake patterns of the wings and tail of hovering hummingbirds. *Exp. Fluids* **46**, 835–846. (doi:10.1007/s00348-008-0602-5)
35. Tritico HM, Cotel AJ. 2010 The effects of turbulent eddies on the stability and critical swimming speed of creek chub (*Semotilus atromaculatus*). *J. Exp. Biol.* **213**, 2284–2293. (doi:10.1242/jeb.041806)
36. Parnaudeau P, Carlier J, Heitz D, Lamballais E. 2008 Experimental and numerical studies of the flow over a circular cylinder at Reynolds number 3900. *Phys. Fluids* **20**, 085101. (doi:10.1063/1.2957018)
37. Prasad A, Williamson CHK. 1997 Three-dimensional effects in turbulent bluff-body wakes. *J. Fluid Mech.* **343**, 235–265. (doi:10.1016/S0894-1777(96)00107-0)
38. Clark CJ, Dudley R. 2010 Hovering and forward flight energetics in Anna's and Allen's hummingbirds. *Physiol. Biochem. Zool.* **83**, 654–662. (doi:10.1086/653477)
39. Bowlin MS, Wikelski M. 2008 Pointed wings, low wingloading and calm air reduce migratory flight costs in songbirds. *PLoS ONE* **3**, e2154. (doi:10.1371/journal.pone.0002154)
40. Smith DL, Brannon EL, Odeh M. 2005 Response of juvenile rainbow trout to turbulence produced by prismatic shapes. *Trans. Am. Fish Soc.* **134**, 741–753. (doi:10.1577/T04-069.1)
41. Cotel AJ, Webb PW, Tritico H. 2006 Do brown trout choose habitats with reduced turbulence? *Trans. Am. Fish Soc.* **135**, 610–619. (doi:10.1577/T04-196.1)